INSTITUTE OF PHYSICS PUBLISHING NETWORK: COMPUTATION IN NEURAL SYSTEMS

Network: Comput. Neural Syst. **12** (2001) 215–233 www.iop.org/Journals/ne PII: S0954-898X(01)23402-2

# Precision of pulse-coupled networks of integrate-and-fire neurons

**P H E Tiesinga[1,4] and Terrence J Sejnowski[1,2,3]**

[1] Sloan–Swartz Center for Theoretical Neurobiology and Computational Neurobiology Laboratory, Salk Institute, 10010 N Torrey Pines Rd, La Jolla, CA 92037, USA
[2] Howard Hughes Medical Institute, Salk Institute, La Jolla, CA 92037, USA
[3] Department of Biology, University of California—San Diego, La Jolla, CA 92093, USA

E-mail: tiesinga@salk.edu

Received 5 September 2000

**Abstract**

Some sensory tasks in the nervous system require highly precise spike trains to be generated in the presence of intrinsic neuronal noise. Collective enhancement of precision (CEP) can occur when spike trains of many neurons are pooled together into a more precise population discharge. We study CEP in a network of $N$ model neurons connected by recurrent excitation. Each neuron is driven by a periodic inhibitory spike train with independent jitter in the spike arrival time. The network discharge is characterized by $\sigma_W$, the dispersion in the spike times within one cycle, and $\sigma_B$, the jitter in the network-averaged spike time between cycles. In an uncoupled network $\sigma_B \sim 1/\sqrt{N}$ and $\sigma_W$ is independent of $N$. In a strongly coupled network $\sigma_B \sim 1/\sqrt{\log N}$ and $\sigma_W$ is close to zero. At intermediate coupling strengths, $\sigma_W$ is reduced, while $\sigma_B$ remains close to its uncoupled value. The population discharge then has optimal biophysical properties compared with the uncoupled network.

## 1. Introduction

The nervous system is capable of producing extremely precise periodic electrical discharges necessary for sensory tasks such as electroreception. As an example of this phenomenal precision, the coefficient of variation (CV)—the standard deviation of the period divided by the mean period—is $\sim 10^{-4}$ for the electric organ discharge generated by the pacemaker nucleus in weakly electric fish [1]. This discharge is produced by a network consisting of 100–150 neurons sparsely connected by electric gap junctions and possibly by chemical synapses. There are two types of neuron in the network, pacemaker cells and relay cells. It is not known how networks of neurons can generate highly precise spike trains in the presence of intrinsic noise [2, 3]. One possible strategy is to pool the discharge of many neurons into a more precise population discharge [4, 5]. This would reduce the jitter in the average spike

[4] To whom correspondence should be addressed.

Here we assume that $I_0 > 0$ and define $t_2$ to be equal to $t_1$ when $V_n = 1$. We then find all the inhibitory pulses that arrive between $t_1$ and $t_2$ and update the membrane potential to the time immediately after pulse arrival (at $t_p^n$ for the $n$th neuron):

$$V_n' = \mathrm{e}^{-(t_p^n - t_1)}(V_n - I_0) + I_0 - p. \tag{8}$$

There may be multiple pulses per neuron, but for simplicity the above notation does not reflect this. Then, all of the neurons are updated to $t_2$: neurons that received inhibitory pulses,

$$V_n'' = \mathrm{e}^{-(t_2 - t_p^n)}(V_n' - I_0) + I_0, \tag{9}$$

and the ones that did not,

$$V_n'' = \mathrm{e}^{-(t_2 - t_1)}(V_n - I_0) + I_0. \tag{10}$$

We then determine which neurons actually crossed the threshold, $V_i'' > 1$, reset their voltage to zero, and emit an excitatory pulse to all neurons. We again check which neurons reached threshold, then their membrane potential is reset to 1 so they would spike immediately, $t_2 = t_1$, in the next iteration of equation (7). This algorithm leads to a large speed-up compared with direct integration using the Runge–Kutta algorithm [9]. In addition, it predicts to machine precision the spike time, whereas for direct integration the spike time is a multiple of the integration time step (see also [10]).

### 2.4. *Calculated quantities*

From the set of spike times $t_i^n$ we compute the phases $\psi_i^n \equiv \mathrm{mod}(t_i^n, T)$, where $t_i^n$ is the $i$th spike time of the $n$th neuron. The temporal and network average of the spike-time jitter is

$$\sigma_\psi^2 = \frac{1}{NM} \sum_{n=1}^{N} \sum_{m=1}^{M} \sum_{i(n,m)} (\psi_i^n)^2 - \mu^2, \tag{11}$$

where the mean phase is

$$\mu = \frac{1}{NM} \sum_{n=1}^{N} \sum_{m=1}^{M} \sum_{i(n,m)} \psi_i^n. \tag{12}$$

Here $N$ is the number of neurons in the network, and $M$ the number of cycles in the simulation run after a transient, $\sum_n$ is the sum over all neurons, $\sum_m$ is the sum over all cycles and $\sum_{i(n,m)}$ is the sum over all spikes $i$ of neuron $n$ that occurred on cycle $m$ *normalized* by the number of these spikes. (Note that on some cycles neuron $n$ may not produce any spikes, whereas during 1:1 entrainment we have the identity $i(n, m) = m$.) The jitter $\sigma_\psi$ is the sum of two contributions,

$$\sigma_\psi^2 = \sigma_W^2 + \sigma_B^2. \tag{13}$$

Here we used the following definitions:

$$\sigma_W^2 = \frac{1}{M} \sum_{m=1}^{M} \sigma_m^2, \tag{14}$$

$$\sigma_B^2 = \frac{1}{M} \sum_{m=1}^{M} \mu_m^2 - \mu^2, \tag{15}$$

and

$$\mu_m = \frac{1}{N} \sum_{n=1}^{N} \sum_{i(n,m)} \psi_i^n, \tag{16}$$

$$\sigma_m^2 = \frac{1}{N} \sum_{n=1}^{N} \sum_{i(n,m)} (\psi_i^n)^2 - \mu_m^2. \tag{17}$$

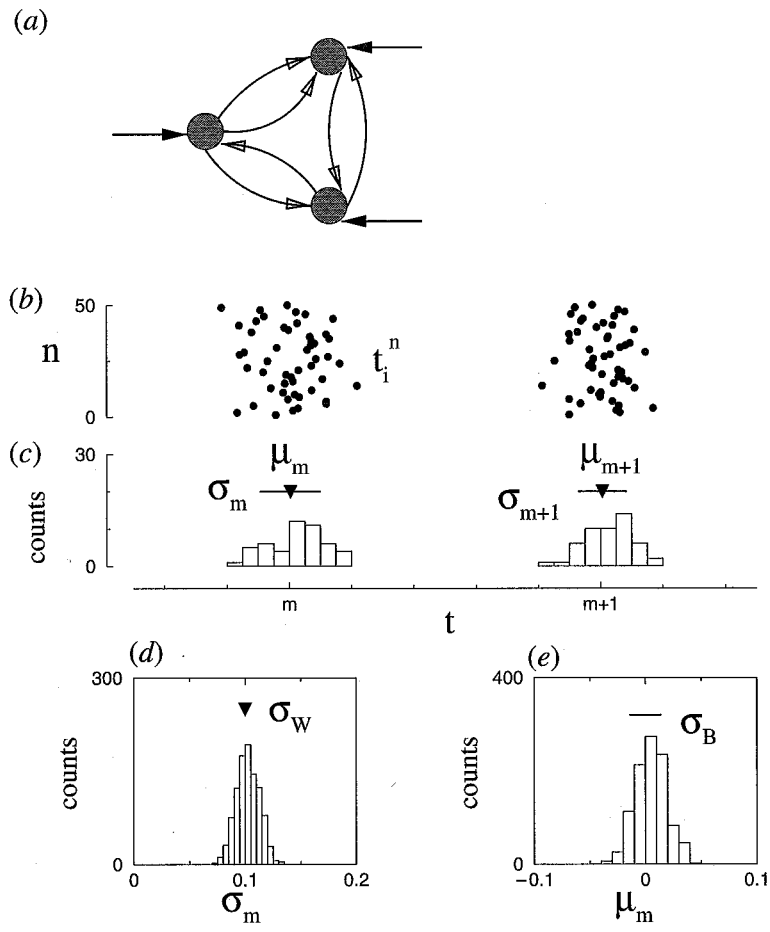


**Figure 1.** Illustration showing the calculation of $\sigma_B$ and $\sigma_W$. (*a*) Schematic diagram of the network model consisting of IAF neurons coupled all-to-all with excitatory synapses (open arrows) and driven by inhibitory inputs (filled arrows). (*b*) Rasterplot for cycles $m$ and $m+1$; the $i$th spike time of the $n$th neuron is shown as a filled circle with its index $n$ as $y$-ordinate and its spike time $t_i^n$ as $x$-ordinate. (*c*) Histogram of spike times; $\mu_m$ (filled triangle) is the average, and $\sigma_m$ (solid line) is the standard deviation of all the spikes during cycle $m$. (*d*) Histogram of $\sigma_m$; $\sigma_W$ (solid triangle) is the average of this distribution. (*e*) Histogram of $\mu_m$; $\sigma_B$ (solid line) is the standard deviation of this distribution.

The calculation of $\sigma_W$ and $\sigma_B$ is illustrated in figure 1. $\sigma_W$ measures the jitter around the average phase in a particular cycle. If the network is fully synchronized—all the neurons fire approximately at the same time in each cycle—$\sigma_W$ will approach zero. In contrast, $\sigma_B$ measures the variation of the average spike phase $\mu_m$ in a particular cycle. It varies as $\sigma_B \sim 1/\sqrt{N}$ for uncoupled neurons (equation (26)). The precision of the population discharge is given by $1/\sigma_B \sim \sqrt{N}$, and increases with increasing $N$. The definition of the phase has a discontinuity: once a phase changes from say 0.99 to 1.01 it is mapped to 0.01. This means that a unimodal distribution of phases centred near 1 would be mapped to two peaks, leading to a higher variance. To prevent this the pulses are applied at $\phi = 0.8$.

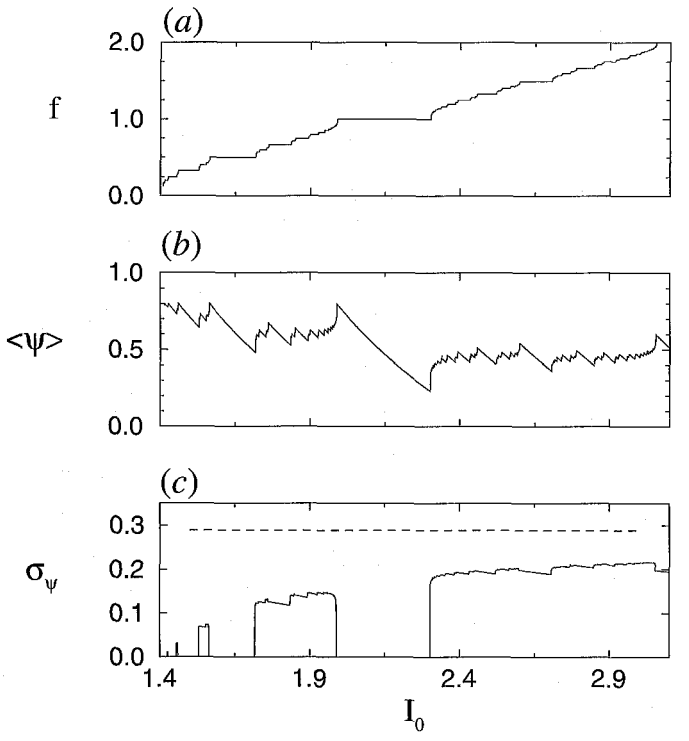


**Figure 2.** Phase locking of an IAF neuron to an inhibitory pulse train. (*a*) The firing rate $f$, (*b*) the average spike phase $\langle\psi\rangle$ and (*c*) the output jitter $\sigma_\psi$ as a function of current $I_0$. The dashed line in (*c*) indicates the standard deviation, $1/\sqrt{12}$, when the phases are uniformly distributed between zero and one. We use the following parameter values: $p = 0.7$; $\sigma_\phi = 0$; $\phi = 0.8$. The averages are over $10 \times 10^3$ cycles, after discarding the initial 200 cycles.

## 3. Results

### *3.1. Single neuron with zero input jitter*

The firing rate versus current ($f$–$I$) characteristic of a current-driven IAF neuron is

$$f = \frac{1}{\ln \frac{I_0 - V_0}{I_0 - 1}}. \tag{18}$$

The neuron does not spike for currents $I_0 < 1$. For currents $I_0 > 1$ the firing rate increases smoothly with increasing current. Here we consider an IAF neuron driven by a periodic inhibitory pulse train with $I_0 > 1$. The emitted spike train can then be entrained, or phase locked, to the input. This leads to steps in the $f$–$I$ characteristic (figure 2(*a*)). On a step the firing rate is constant for a range of current values, and equal to a fraction $\frac{n}{m}$ of the driving frequency (here $n$ and $m$ should not be confused with the neuron and cycle index, respectively). The neuron emits $n$ spikes in $m$ cycles of the drive. We now focus on the 1:1 ($n = 1, m = 1$) step located between $I_0 = 2.0$ and 2.3 for $p = 0.7$. The pulse arrives each cycle at phase $\phi = 0.8$, and the neuron spikes each cycle at phase $\psi$. At the left-hand side of the step the neuron spikes shortly before the arrival of the next inhibitory pulse. For increasing current the neuron spikes earlier, and $\psi$ decreases (figure 2(*b*)).

The precision of a single neuron is the inverse of the standard deviation $\sigma_\psi$ of the spike phase. A larger $\sigma_\psi$ thus means a lower precision. In figure 2(*c*) we plot $\sigma_\psi$ versus current. It is zero on the 1:1 and 1:*m* steps and it is nonzero outside these steps.

### *3.2. Single neuron with input jitter*

Now consider the case when the inhibitory pulses arrive with a temporal jitter $\sigma_\phi$. Their arrival phase $\phi_m$ is independent in each cycle, and distributed according to Gaussian probability distribution with mean $\phi$, and variance $\sigma_\phi^2$. In this subsection we again have suppressed the neuron index $n$. The input jitter introduces jitter in the output spike train on the 1:1 step. The spike time in the $m$th cycle is $t_m = mT + \psi_m$. The spike phase $\psi_m$ jitters around its stationary value $\psi$ according to equation (4),

$$\psi_{m+1} = \psi_m + \ln\left[a(V_0) + b\mathrm{e}^{\Delta\phi_m - \psi_m}\right] - T. \tag{19}$$

Note that $a$ and $b$ were defined in equations (5) and (6), $\Delta\phi_m$ is the jitter in the pulse arrival time.

Given the distribution of the input jitter,

$$P_{\Delta\phi}(\Delta\phi_m) = \frac{1}{\sqrt{2\pi\sigma_\phi^2}} \exp\left(-\frac{\Delta\phi_m^2}{2\sigma_\phi^2}\right), \tag{20}$$

and the value of the previous phase $\psi_m$, the distribution of the next phase $\psi_{m+1}$ is

$$Q(\psi_{m+1}|\psi_m) = J(\psi_{m+1}) P_{\Delta\phi}\left(\ln\frac{\mathrm{e}^{T+\psi_{m+1}} - a\mathrm{e}^{\psi_m}}{b}\right). \tag{21}$$

Here we used

$$J(\psi_{m+1}) = \frac{\mathrm{d}\Delta\phi_m}{\mathrm{d}\psi_{m+1}} = \frac{\mathrm{e}^{T+\psi_{m+1}}}{\mathrm{e}^{T+\psi_{m+1}} - a\mathrm{e}^{\psi_m}}.$$

Equation (21) is obtained by inverting equation (19) to express $\Delta\phi_m$ as function of $\psi_{m+1}$, and then multiplying the $P_{\Delta\phi}$ by the Jacobian $J$. The distribution for $\psi_m$ in cycle $m$ is obtained by iterating the following equation starting from a distribution $P_0$ for the starting phase difference $\psi_0$:

$$P_{m+1}(\psi_{m+1}) = \int \mathrm{d}\psi_m \, Q(\psi_{m+1}|\psi_m) P_m(\psi_m).$$

In numerical simulations the distribution $P_m(\psi_m)$ converged to a stationary distribution $P_\mathrm{s}$. We have not established whether this holds for all parameters and initial conditions. The stationary distribution is a solution of

$$P_\mathrm{s}(t) = \int \mathrm{d}s \, Q(t|s) P_\mathrm{s}(s). \tag{22}$$

Equation (22) turns into a matrix equation $P_j = \sum_i Q_{ij} P_j$ when $\psi$ takes discrete values labelled by the indices $i$ and $j$. The stationary distribution then corresponds to the eigenvector at eigenvalue $\lambda = 1$. We numerically determined the stationary distribution using Matlab (MathWorks). For small jitter, $\sigma_\phi \ll T$, one can instead linearize equation (19) in terms of the small deviations $\Delta\psi_m = \psi_m - \psi$. To simplify, without loss of generality, we have chosen $\phi$ such that $\psi = 0$ (see section 2), yielding

$$\Delta\psi_{m+1} = \frac{a}{a+b}\Delta\psi_m + \frac{b}{a+b}\Delta\phi_m. \tag{23}$$

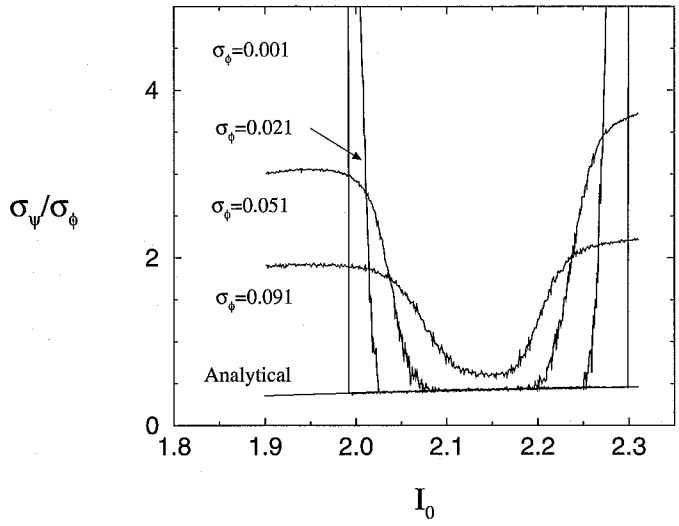


**Figure 3.** Output spike jitter $\sigma_\psi$ normalized by the input jitter $\sigma_\phi$ as a function of current on the 1:1 entrainment step for $\sigma_\phi = 0.001$, 0.021, 0.051 and 0.091 as labelled. The solid curve is the analytical curve from of equation (24). We use $p = 0.7$ and $\phi = 0.8$. The averages are over $50 \times 10^3$ cycles, after discarding the initial $2 \times 10^3$ cycles.

After an initial transient the distribution of $\Delta\psi_n$ converges to a stationary distribution. Hence the moments of the distribution in consecutive cycles are the same, $\langle \Delta\psi_{m+1}^2 \rangle = \langle \Delta\psi_m^2 \rangle$. Together with equation (23) this yields the following expression for the output jitter as a function of the input jitter:

$$\sigma_\psi^2 = \langle \Delta\psi_m^2 \rangle = \frac{\langle \Delta\phi_m^2 \rangle}{1 + 2a(0)/b} \equiv c_0^2 \sigma_\phi^2. \tag{24}$$

The above equation defines the proportionality constant $c_0$. The average and variances of the numerically determined distribution $P_s$ are in excellent agreement with equation (24) for $\sigma_\phi < 0.05$ (not shown).

We also performed direct simulations based on equation (1) for different values of $\sigma_\phi$ (with parameters values $N = 1$ and $g = 0$). We plot in figure 3 the output jitter as a function of current on the 1:1 step, together with the results of equation (24). The numerical simulations only agree with the analytical expression for current values in the middle of the step. The width of this region decreases with increasing input jitter, and disappears for $\sigma_\phi > 0.05$. In order to understand why the analytic expression fails near the edges of the step we examine how the phase locking on the 1:1 step becomes unstable for low and high currents. For low currents, near the left-hand edge of the step, the neuron spikes just before the arrival of the next inhibitory pulse. If the current were reduced even more, the pulse would arrive before the spike is emitted. This would delay the spike even further into the next cycle. Therefore we have a cycle without any spikes: the neuron has skipped a cycle. Skipping destabilizes the phase locking. Due to jitter the inhibitory pulse can arrive before the neuron would spike, even on the entrainment step. The neuron will then spike in the next cycle, but at a phase far from its average value $\psi$. It takes a few cycles to return to its stationary value. The skipping leads to extra output jitter that is not accounted for in our analytical treatment.

The time series of the spike phases and the resulting return map is shown in figure 4. The time series for $I_0 = 2.15$ (the middle of the step) consists of small deviations around the

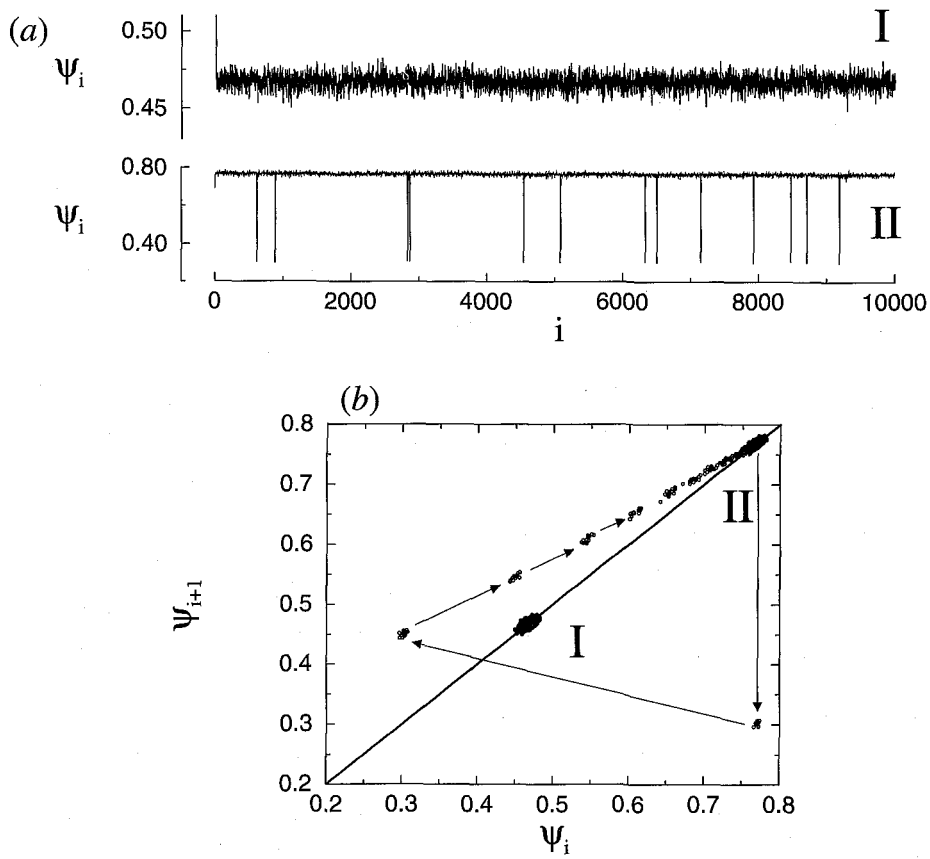


**Figure 4.** Spike skipping near the right-hand edge of the 1:1 entrainment step. (*a*) The spike phase versus index $i$; (*b*) the return map (the phase $\psi_{i+1}$ versus the phase $\psi_i$). The solid line is $\psi_{i+1} = \psi_i$. The location of the fixed point of the map is given by its intersection with the solid line. The arrows indicate the temporal progression of the dynamics after a skip. Here (I) $I_0 = 2.15$ and (II) $I_0 = 2.0028$ with $p = 0.7$, $\phi = 0.8$ and $\sigma_\phi = 0.01$.

average $\psi = 0.47$. In the return map we plot the phase $\psi_{i+1}$ versus the previous phase $\psi_i$: it consists of a compact cluster of dots. In contrast, the time series for $I_0 = 2.0028$ ($\psi = 0.77$) is characterized by infrequent large deviations when the neuron skips a cycle. During skipping the phase jumps from $\psi_i \approx 0.77$ to 0.3, then it returns to 0.77 over the next few cycles. The return map now consists of multiple clusters of points.

On the right-hand edge of the current step the neuron spikes long before the next inhibitory pulse arrives. For an even higher value of the current the neuron can spike again before the pulse arrives. In that case there are two spikes in one cycle, and the next spike will happen at a phase far from the fixed-point phase. In this way the phase locking becomes unstable. In the presence of jitter the inhibitory pulse can arrive at a later time, and therefore the neuron can spike twice in one cycle even on the entrainment step. This leads to increased output jitter in an analogous fashion to skipping.

To summarize, the output jitter attains its minimum on the entrainment step. There it is linearly proportional to the input jitter. The width of the linear region decreases for increasing input jitter.

### 3.3. Uncoupled network

For the uncoupled network the average spike time $\mu_m$ is the sum of $N$ independent variables $\psi_m^n$, each satisfying equation (19), and with standard deviation $\sigma_\psi$. (The phase distribution is not Gaussian, though for small $\sigma_\phi$ it is a good approximation.) Hence, for large $N$, using the law of large numbers [8], the standard deviation of $\mu_m$ will approach

$$\sigma_B = \frac{\sigma_\psi}{\sqrt{N}}, \tag{25}$$

and since the distribution of all the phases is the same as the distribution of each individual phase, $\sigma_W \approx \sigma_\psi$.

On the entrainment step $\sigma_\psi \approx c_0\sigma_\phi$, hence

$$\sigma_B \approx \frac{c_0\sigma_\phi}{\sqrt{N}}. \tag{26}$$

These results are confirmed using direct simulation of the ensemble of neurons in the next subsection.

### 3.4. Strongly coupled network

We now discuss the dynamics of a network of IAF neurons coupled all-to-all via excitatory pulses. Previously it was shown that excitatory coupling can lead to synchronization [11–14]. Here, each neuron in addition receives the same periodic inhibitory pulse train. However, the jitter in the pulse arrival time is uncorrelated between different neurons. This network converges for strong enough coupling to a synchronized state in which all neurons fire at the same time. Just after the neurons fire, they each receive $N$ excitatory pulses of strength $g/N$. This instantaneously increases the membrane potential from its reset value 0 to $g$. In the time interval just after the last spike and just before the next spike there are no other excitatory pulses, hence the dynamics of each network neuron is reduced to equation (4), with initial condition $V_0 = g$. In the absence of input jitter all neurons have identical dynamics and thus the network spike times are also given by equation (4). Once again there are phase-locked solutions, including the 1:1 entrainment step. The position of the step is shifted to lower current values due to the excitatory coupling. However, because of the coupling the effects of the input jitter are different from before. The first neuron to spike will emit pulses to other neurons. As a result they will all spike earlier. If the coupling is strong enough and the voltage distribution is sharp enough, the first spike will make all other neurons spike immediately afterwards. The network spike times are thus given by the earliest spike time of an ensemble of noisy uncoupled neurons.

In equation (4), $\psi_{m+1}$ increases as a function of $\Delta\phi_m$, therefore the earlier the inhibitory pulse arrives, the sooner the neuron spikes. Since in the synchronized state all neurons have the same membrane potential, the neuron that receives the earliest inhibitory pulse will spike first. The distribution of earliest pulse times is equal to the distribution $P_{\min}(\Delta\phi_m^{\min})$ of the minimum $\Delta\phi_m^{\min}$ of $N$ randomly drawn deviates $\Delta\phi_m^n$ from a Gaussian probability distribution. The analytical expression for $P_{\min}$ and the asymptotic values of its first and second moment are given in the appendix. The dynamics of the synchronized spike phase of the whole network is thus given by equation (4) driven by a pulse train with jitter $\Delta\phi_m^{\min}$. The distribution $P_{\min}$ is different from $P_{\Delta\phi}$ in two ways. First, the average $\langle\Delta\phi_m^{\min}\rangle$ is nonzero. The expected value for the minimum of $N$ deviates with average zero is negative, asymptotically $\langle\Delta\phi_m^{\min}\rangle \sim -\sqrt{\log N}$. Second, the distribution is more sharply peaked; the standard deviation scales asymptotically as $\sigma_{\text{eff}} \sim \sigma_\phi/\sqrt{\log N}$. The distribution is asymmetric: the tail on the left-hand side is longer than the one on the right-hand side. We can now repeat the analysis done on equation (19) with

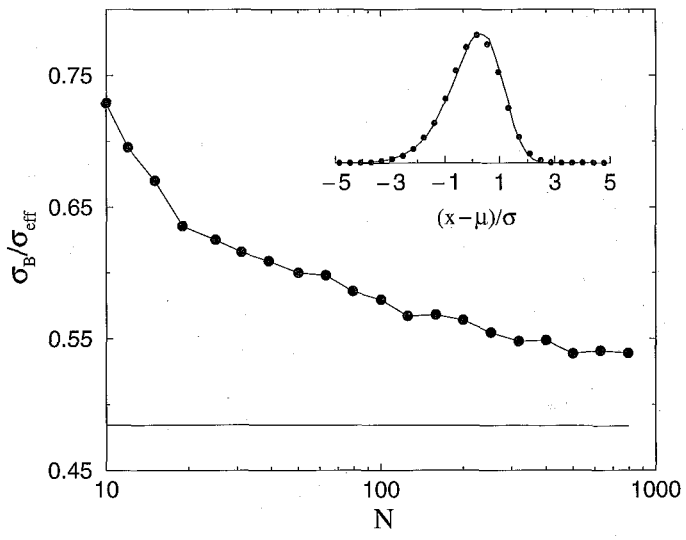


**Figure 5.** Output spike jitter $\sigma_B$ normalized by $\sigma_{\text{eff}}$ (filled circles) and the analytical result equation (24) (solid curve). In the inset we plot the distribution of $\mu_m$ (circles) and of $\Delta\phi_m^{\min}$ (solid curve). The $x$-ordinate is scaled so both distributions have zero mean and unit variance. Here $g = 0.4$, $p = 0.7$, $\phi = 0.8$ and $\sigma_\phi = 0.01$. Averages are over $80 \times 10^3$ cycles, after discarding the initial 200 cycles.

input jitter according to the new distribution $P_{\min}$. The spike times generated by equation (19) are now the spike times of the network, instead of those of a single neuron. There was good agreement between results obtained by discretizing equation (22) and those obtained by linearization of equation (19), $\sigma_\psi = c_g\sigma_\phi$, $c_g = \frac{1}{1+2a(V_0=g)/b}$ (not shown). Since the earliest pulse $\Delta\phi_m^{\min}$ arrives on average at phase $\phi' = \phi + \langle\Delta\phi_m^{\min}\rangle$ we use $\phi'$ instead of $\phi$ in equation (6) for $b$. We have also determined using simulations of the full network the distribution of $\Delta\phi_m^{\min}$ and the average spike phase $\mu_m$ (see equation (16)). We rescaled them by their average $\mu$ and variance $\sigma$: $y = (x-\mu)/\sigma$ with $x = \Delta\phi_m^{\min}$ (or $\mu_m$) and plotted them both in figure 5. The two distributions have approximately the same shape. The ratio $\sigma_\psi/\sigma_{\text{eff}}$ obtained from simulations comes closer to the theoretical value $c_g$ as $N$ increases. We did not establish whether $\sigma_\psi/\sigma_{\text{eff}}$ would converge to $c_g$ for even larger $N$. The analytical result only yields qualitatively correct results for the network sizes studied here and it should be interpreted as a lower bound for $\sigma_\psi$.

We now describe the results of the simulations of the full network in more detail. In figure 6 we compare the behaviour of the precision as a function of $N$ for two different current values, $I_0 = 1.77$, close to the left-hand edge of the step, and $I_0 = 1.88$ in the middle of the step. In the middle of the step $\sigma_B$ only decreases very slowly with increasing $N$. It provides the largest part of $\sigma_\psi$. The jitter $\sigma_W$ starts out at values close to zero for a small network with $N = 10$. This means that the network is almost fully synchronized. However $\sigma_W$ increases with system size, and levels off for $N > 100$. For larger networks the effect of a single excitatory pulse, $g/N$, is not strong enough to immediately bring all other neurons to threshold, leading to dispersion in the spike times within a cycle. The average arrival phase of the first pulse is $\phi + \langle\Delta\phi_m^{\min}\rangle$ (the average is over the cycles $m$). The earliest inhibitory pulse moves to an earlier phase for increasing $N$, hence the spike phase $\mu$ also moves to earlier times (figure 6($f$)).

Next, consider the edge of the step. The jitter $\sigma_B$ decreases quickly with increasing $N$ (figure 6($a$)). In this case the largest contribution to $\sigma_\psi$ is given by $\sigma_W$ (figure 6($c$)).

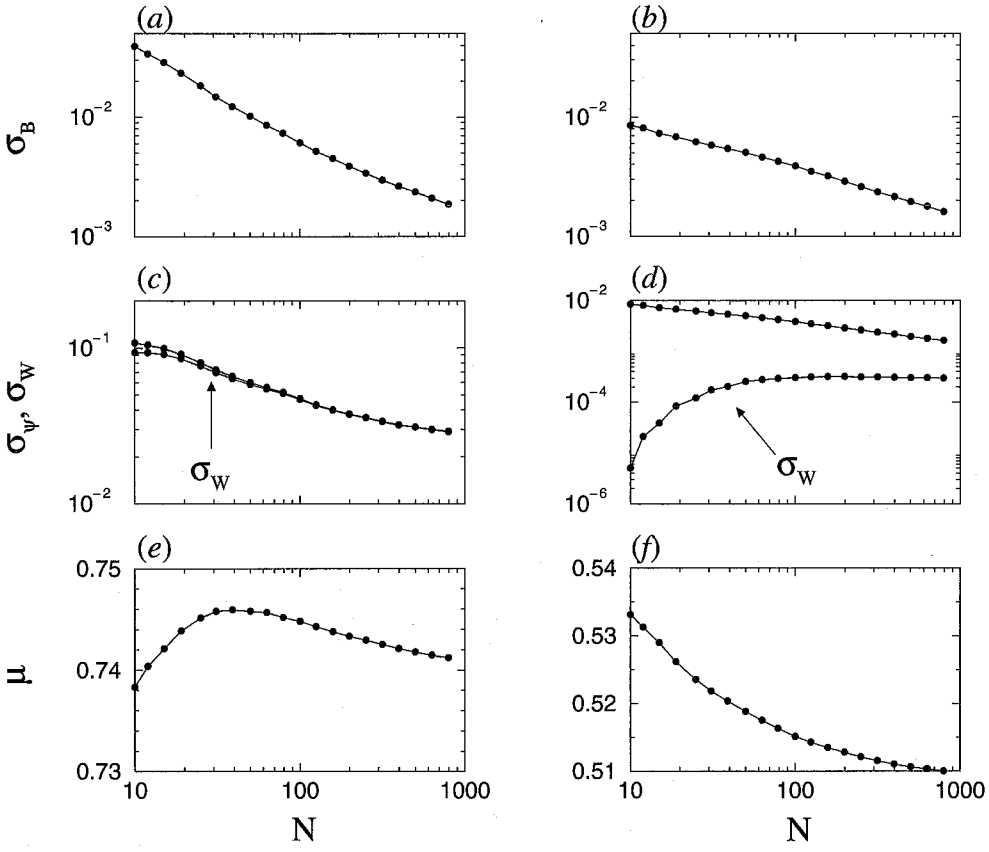


**Figure 6.** Precision as a function of network size, $N$. Plots of $(a)$, $(b)$ $\sigma_B$, $(c)$, $(d)$ $\sigma_W$ and $\sigma_\psi$ and $(e)$, $(f)$ $\mu$ versus $N$ (definitions are given in the section 2). Here $(a)$, $(c)$, $(e)$ $I_0 = 1.77$, and $(b)$, $(d)$, $(f)$ $I_0 = 1.88$. The other parameters are $g = 0.4$, $p = 0.7$, $\phi = 0.8$ and $\sigma_\phi = 0.01$. Averages are over $40 \times 10^3$ cycles, after discarding the initial 200 cycles.

The decrease in $\sigma_\psi$ is therefore due to an increase in synchronization as measured by $\sigma_W$. Interestingly, $\mu$ depends nonmonotonically on $N$ (figure 6$(e)$). To understand this in more detail we study the time trace of the phase of one individual neuron in the network for $N = 10$ and 79 (figures 7$(a)$ and $(b)$). The time series consists of small deviations from the average, interspersed with large deviations due to skipping. The frequency of skipping depends on network size: for $N = 10$ it occurs more frequently compared with $N = 79$. Skipping increases the value of $\sigma_W$ and $\sigma_B$. We have also plotted the probability distribution of the spike phase, with the large deviations excluded (figures 7$(c)$, $(d)$). Two features change when increasing $N$. The mean of the distribution moves away from $\phi = 0.8$, and the distribution becomes sharper. These two changes make it harder for skipping to occur in larger networks. The increase in precision with $N$ near the edge is therefore partly due to the suppression of skipping, and partly due to the reduced jitter in $\Delta\phi_m^{\min}$.

We now investigate how the increase in precision of a strongly coupled network compares to that in uncoupled networks. There are two questions to be addressed. Firstly, how does the precision increase with $N$ compared with the initial precision at a small network size (here $N = 10$)? We therefore plot $\sigma_B(N)/\sigma_B(10)$ versus $N$ in figures 8$(a)$ and $(b)$. In the middle

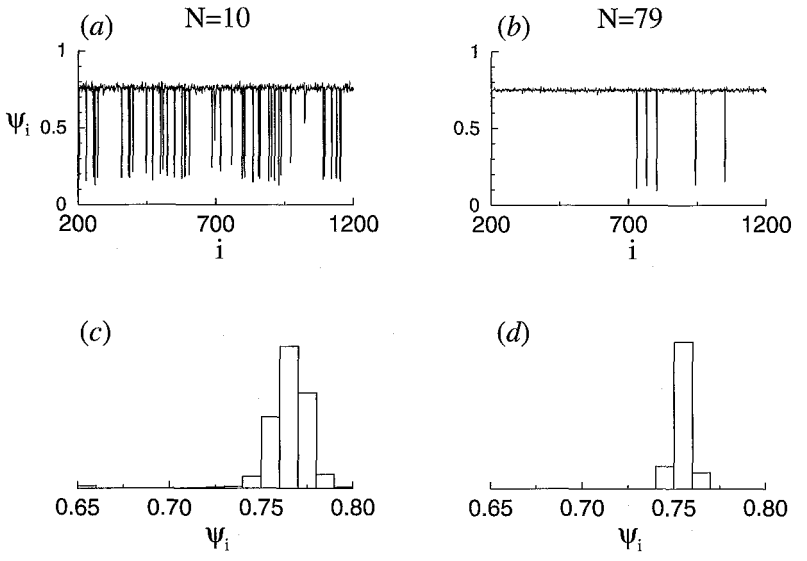


**Figure 7.** The spike phase and its probability distribution. Plots of (*a*), (*b*) the spike phase $\psi_i$ versus index $i$, and (*c*), (*d*) its distribution with large deviations ($\psi_i < 0.6$) excluded. Here $N = 10$ (*a*), (*c*) and $N = 79$ (*b*), (*d*), and $g = 0.4$, $p = 0.7$, $\phi = 0.8$, $\sigma_\phi = 0.01$.

part of the step the precision of the uncoupled network increases faster with $N$ than in the coupled network (figure 8(*a*)). However, near the edge the coupled network performs better than the uncoupled network (figure 8(*b*)). The second question is how the output jitter $\sigma_B$ varies with $N$, compared with the input jitter $\sigma_\phi$. In figures 8(*c*) and (*d*) we therefore plot $\sigma_B/\sigma_\phi$. We find that the uncoupled network always has a higher precision compared with a strongly coupled network. Near the edge of the step the coupled network performs almost an order of magnitude worse compared with the uncoupled network.

### *3.5. Precision for intermediate strength of the coupling*

In figure 9 we show the crossover in the precision from its value in the uncoupled network to its value in the strongly coupled network. The spike phase shifts to earlier times in the cycle when $g$ is increased at a fixed current. To allow for an unbiased comparison we decrease the current as a function of $g$ to keep the fixed-point spike phase $\psi$ constant. We first discuss the results for $\sigma_\phi = 0.005$. The roman numerals refer to the labels in figure 9. (I) $\sigma_W$ and $\sigma_B$ remain constant up to $g \sim 10^{-4}$. (II) For values between $g \sim 10^{-4}$ and $g \sim 10^{-2}$, $\sigma_W$ decreases sharply, but $\sigma_B$ remains approximately equal to its $g = 0$ value. (III) For $g > 10^{-2}$, the decrease in $\sigma_W$ is reduced, but $\sigma_B$ increases. At $g \sim 1$, the strongly coupled limit is reached: $\sigma_W$ is close to zero.

The onset of the decrease in $\sigma_W$ (II) shifts to higher coupling strengths for increasing $\sigma_\phi$. The increase in $\sigma_B$ (III) is still coupled to the levelling off of the decrease in $\sigma_W$. However, at higher coupling strength (IV) the phase locking becomes unstable: both $\sigma_W$ and $\sigma_B$ increase.

To summarize, at intermediate coupling strengths $\sigma_B$ stays close to its optimal $g = 0$ value, but $\sigma_W$ can be reduced by increasing $g$. The quantities $\sigma_B\sqrt{N}/\sigma_\phi$ and $\sigma_W/\sigma_\phi$ saturate as a function of $N$ for $N > 79$ (not shown).

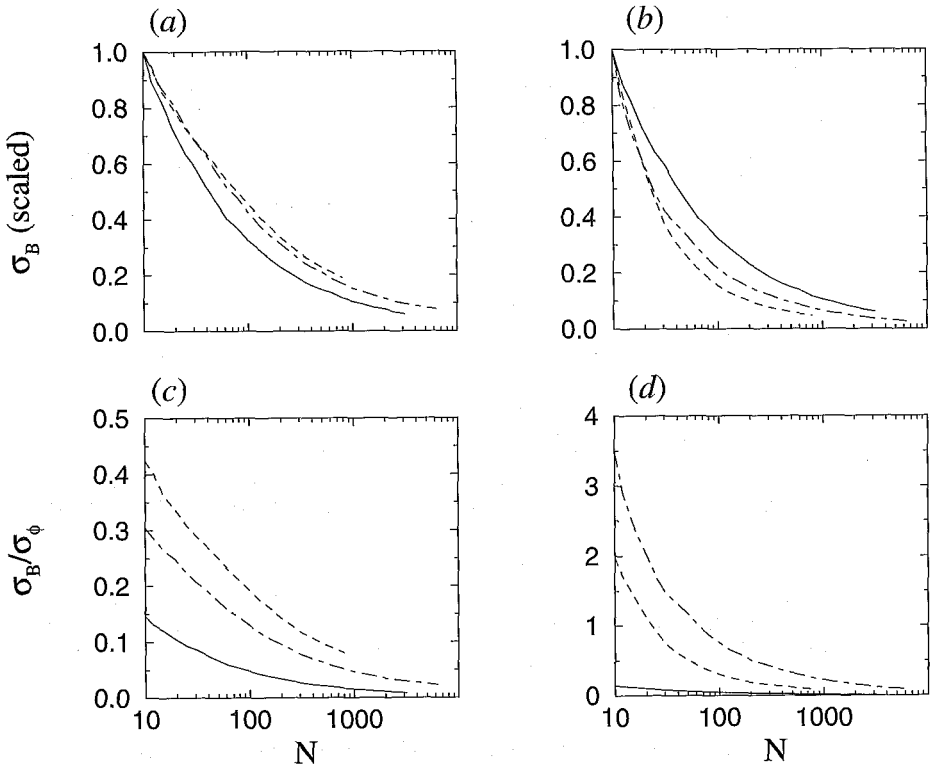


**Figure 8.** Scaling of precision with network size. Plots of (*a*), (*b*) $\sigma_B(N)/\sigma_B(10)$ and (*c*), (*d*) $\sigma_B(N)/\sigma_\phi$ versus network size $N$. The reference curve (solid curve) for an uncoupled network at $I_0 = 2.15$ is the same in all panels. Results are shown for two coupling constants $g = 0.1$ (dot–dashed curve) and $g = 0.4$ (dashed curve). In (*a*) and (*c*) the current is in the middle of the entrainment step, $I_0 = 1.97$ ($g = 0.1$) and $I_0 = 1.88$ ($g = 0.4$), whereas in (*b*) and (*d*) the current value is on the left-hand side of the step, $I_0 = 1.934$ ($g = 0.1$) and $I_0 = 1.77$ ($g = 0.4$). Other parameters are $p = 0.7$, $\phi = 0.8$ and $\sigma_\phi = 0.01$. Averages are over at least $40 \times 10^3$ cycles, after discarding the initial 200 cycles.

## 4. Discussion

The properties of the discharge of an ensemble of neurons can be measured in a number of different ways. One can pool the spike phases of all the neurons in all cycles together and calculate the variance $\sigma_\psi^2$ of the resulting distribution. This variance contains contributions from two cycle-related variances: $\sigma_W^2$, measuring the average width of the network discharge, and $\sigma_B^2$, measuring the jitter in the timing of the population discharge. Most studies concerned with collective enhancement of precision (CEP) focus primarily on $\sigma_B$. $\sigma_W$ and $\sigma_B$ are both biophysically relevant and here we have carefully studied their behaviour. We now briefly summarize our results for $\sigma_W$ and $\sigma_B$.

An IAF neuron driven by a periodic inhibitory pulse train attains its highest precision (lowest value for $\sigma_\psi$) on $1 : m$ phase-locking steps. The 1:1 step has the largest width and is thus the most stable. In the presence of jitter $\sigma_\phi$ in the arrival times of the inhibitory pulses the highest precision is still obtained on the phase-locking step, but only in the middle, most stable part. There $\sigma_\phi$ and $\sigma_\psi$ are linearly related, $\sigma_\psi = c_0\sigma_\phi$. Skipping occurs close to the edges of the step and it always increases the output jitter. The spike trains of $N$ independent (uncoupled)

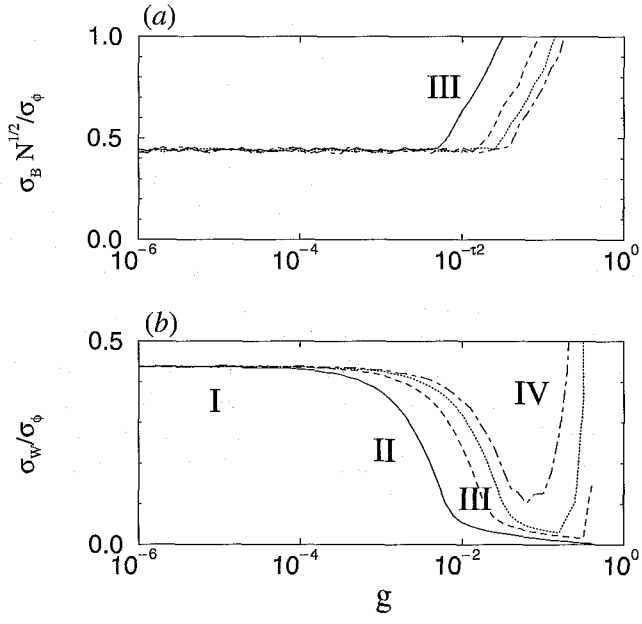


**Figure 9.** Crossover of precision from uncoupled to strongly coupled networks. (*a*) $\sigma_B\sqrt{N}/\sigma_\phi$ and (*b*) $\sigma_W/\sigma_\phi$ versus coupling strength $g$ for $\sigma_\phi = 0.005$ (solid curves), 0.015 (dashed curves), 0.025 (dotted curves) and 0.035 (dot–dashed curves), with $p = 0.7$. The current $I_0$ is covaried with $g$ to keep the fixed-point spike phase equal to $\psi = 0.383$. Roman numerals refer to regions of $g$ defined in the text in section 3.5. Averages are over $5 \times 10^3$ cycles, after discarding the initial 100 cycles.

neurons pooled together yield a network discharge with $\sigma_B \approx \sigma_\psi/\sqrt{N}$, and $\sigma_W \approx \sigma_\psi$. The jitter $\sigma_B$ in the network spike times therefore decreases quickly with increasing network size, but the width $\sigma_W$ of the discharge in a given cycle remains unchanged.

For a coupled network the maximal precision is also attained in the middle of the phase-locking step. In a fully synchronized network we have by definition $\sigma_W \approx 0$ and $\sigma_B = c_g\sigma_{\text{eff}}$. $\sigma_{\text{eff}}$ is the variance in the distribution of $\Delta\phi_m^{\min}$, and it scales asymptotically as $\sigma_{\text{eff}} \sim 1/\sqrt{\log N}$. We find numerically that this limit for $\sigma_B$ is not reached, and that this expression should be interpreted as a lower bound. Therefore the CEP, $1/\sigma_B$, in the strongly coupled network is less than that of an uncoupled network.

At intermediate coupling strength there is a crossover in $\sigma_W$ and $\sigma_B$ from the uncoupled values to the strongly coupled values. The onset of the decrease in $\sigma_W$ occurs at a lower coupling strength compared with the increase in $\sigma_B$. As a result there is an optimal value of $g$ where $\sigma_B$ is close to its optimal value (at $g = 0$), whereas $\sigma_W$ is substantially reduced.

What are the functional consequences of these differences between coupled and uncoupled networks? It is desirable to have a low value for $\sigma_W$, since most neurons will spike more reliably when they are driven by a barrage of spikes that are close together in time compared with when there is a large dispersion. During transduction of network spike trains into a continuous electric signal, as occurs in the electric fish, a low $\sigma_W$ would yield a much larger phasic-to-tonic ratio than a spike train with a higher value of $\sigma_W$. Here the limitations of the uncoupled network come to light: no matter how many neurons there are in the network $\sigma_W$ will stay the same and equal to the original jitter in a single neuron. In a coupled network one can find values for $N$ and $g$ that satisfy arbitrary requirements on $\sigma_W$ and $\sigma_B$.

In this study we have investigated how precision increases with network size $N$ using a simple neural model. The model lacks features that are present in physiological systems, such as a time scale for EPSPs and IPSPs, and it produces zero-width action potentials. Furthermore, functionally important synaptic effects such as facilitation and depression were not taken into account [15, 16]. Despite its simplicity the model produces phase-locking steps in the firing rate. Phase locking of neuronal discharge to a periodic injected current, periodic presynaptic spike trains and even synchronized network discharge are ubiquitous in the nervous system. Phase locking has been studied theoretically in IAF neurons [17–20], Fitzhugh–Nagumo models [21] and Hodgkin–Huxley-based models [22]. Recently, it was shown that entrainment or phase locking can lead to a precision resonance [22–24]. Here we investigated how precision resonance in combination with recurrent excitation influences the CEP. We also specifically address the effect of jitter in the input spike train. The main advantage of the present approach is that analytical estimates for large-$N$ networks can be obtained and tested using efficient simulations. However, it is important to determine how our estimates carry over to more biophysically accurate models, which will be the subject of future research.

## Acknowledgments

We thank Daniel Needleman, Alexei Koulakov and Jorge V José for useful comments. We thank the anonymous referees for comments that have improved the paper. Some of the numerical calculations were performed at the High Performance Computer Center at Northeastern University. This research was supported by the Sloan–Swartz Center for Theoretical Neurobiology at the Salk Institute, and the Center for Interdisciplinary Research on Complex Systems at Northeastern University.

## Appendix

The variance of the distribution $P_{\min}$ determines the output jitter of the strongly coupled network. Here we determine the asymptotics of the variance for very large networks to complement the numerical results for small to large networks described in the main body of the text. In the following we determine $P_{\min}$ exactly and then proceed to make a number of approximations to find the first and second moments as a function of network size $N$.

First we calculate the distribution of $\Delta\phi_m^{\min}$, the minimum value of $\Delta\phi_m^n$ in a given cycle $m$, as a function of the network size (for simplicity we use the notation $x = \Delta\phi_m^{\min}$ and $\sigma = \sigma_\phi$). The distribution of the minimum of $N$ independent, identically distributed variables with probability distribution function $P(x)$ and cumulative probability distribution $\delta(x)$ reads [25]

$$P_{\min}(x, N) = NP(x)(1 - \delta(x))^{N-1} \equiv e^{-F}, \tag{27}$$

where

$$P(x) = \frac{1}{\sqrt{2\pi\sigma^2}} \exp\left(-\frac{x^2}{2\sigma^2}\right), \tag{28}$$

is the distribution of the original $x = \Delta\phi_m^n$, and

$$1 - \delta(x) = \int_x^\infty P(y)\,\mathrm{d}y = \frac{1}{2} - \frac{1}{2}\mathrm{erfc}\left(\frac{x}{\sqrt{2}\sigma}\right). \tag{29}$$

There is excellent agreement between $P_{\min}$ determined using numerical simulations and the analytical expression equation (27) (figure A.1($a$)). We expand $\delta$ asymptotically in $1/x$

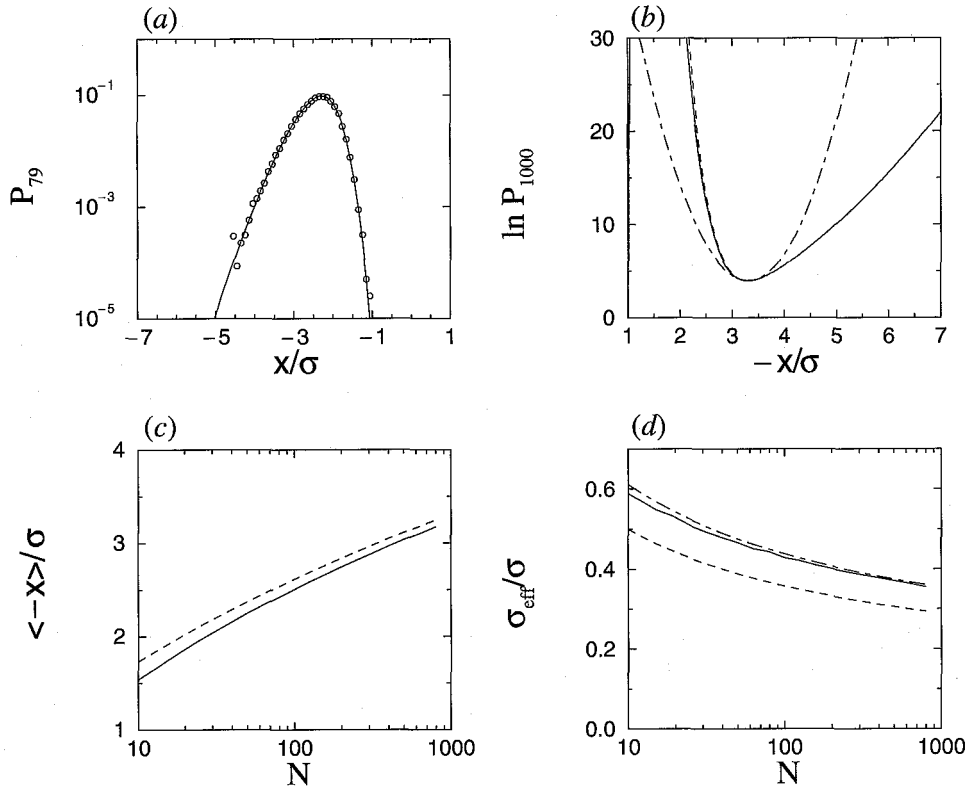


**Figure A.1.** Comparison of simulations to analytical results. (*a*) Distribution of the minimum $x$ obtained from simulations (open circles), and the result of equation (27) (solid curve) for $N = 79$. (*b*) Exponent of equation (27) (continuous curve) compared with the asymptotic expansion equation (31) (dashed curve), and the saddle point expansion equation (35) (dot–dashed curve). (*c*) Average obtained from simulations (continuous curve) compared with the saddle point position $x_0$ (equation (36), dashed curve). (*d*) Standard deviation from simulations (continuous curve) compared with equation (36) (dashed curve). The dot–dashed curve is the dashed curve multiplied by $\sqrt{\frac{3}{2}}$. Averages over $80 \times 10^3$ cycles, after discarding the initial $2 \times 10^3$ cycles.

for large *negative* $x$,

$$\delta(x) \approx -\frac{1}{\sqrt{2\pi}}\frac{\sigma}{x}\mathrm{e}^{-\frac{x^2}{2\sigma^2}}\left(1-\frac{\sigma^2}{x^2}\right). \tag{30}$$

Then, using the approximation $\log 1 - \delta \approx -\delta$, we obtain

$$F(x) \approx \frac{x^2}{2\sigma^2} - (N-1)\frac{1}{\sqrt{2\pi}}\frac{\sigma}{x}\mathrm{e}^{-\frac{x^2}{2\sigma^2}}\left(1-\frac{\sigma^2}{x^2}\right). \tag{31}$$

In figure A.1(*b*) the result of equation (31) to the exact result (equation (27)). We find excellent agreement for $N > 1000$ and $-x/\sigma > 2$. We further approximate the distribution using the saddle point expansion. The first derivative of $F$ is (up to second order in $\frac{\sigma}{x}$)

$$F'(x) = \frac{x}{\sigma^2} + \frac{N-1}{\sigma\sqrt{2\pi}}\mathrm{e}^{-\frac{x^2}{2\sigma^2}}. \tag{32}$$

The minimum of $F$ is located at $x_0$ given by $F'(x_0) = 0$,

$$\frac{x_0}{\sigma} = -\frac{N-1}{\sqrt{2\pi}} e^{-\frac{x_0^2}{2\sigma^2}}. \tag{33}$$

The value of the second derivative at $x_0$ is

$$F''(x_0) = \frac{1}{\sigma^2} - \frac{N-1}{\sqrt{2\pi}} \frac{x_0}{\sigma^3} e^{-\frac{x_0^2}{2\sigma^2}} = \frac{1}{\sigma^2}\left(1 + \frac{x_0^2}{\sigma^2}\right). \tag{34}$$

Using the above results we get for the saddle-point expansion

$$F_{\text{saddle}} = F(x_0) + \tfrac{1}{2}F''(x_0)(x - x_0)^2. \tag{35}$$

In figure A.1($b$) we compare this expression to equations (27) and (31). Equation (35) only yields a good approximation for $x$ values close to $x_0$. The saddle point expansion defines a Gaussian probability distribution with mean $x_0$ and variance $\sigma_{\text{eff}}^2 = 1/F''(x_0)$. For exponentially large $N$, $\ln N \gg 1$, we obtain

$$\begin{aligned} \frac{x_0}{\sigma} &\sim -\sqrt{2\ln(N-1)}, \\ \frac{\sigma_{\text{eff}}^2}{\sigma^2} &\sim \frac{1}{1 + 2\ln(N-1)}. \end{aligned} \tag{36}$$

We have compared these asymptotic estimates to the mean and variance determined by numerical integration of equation (27). The exact results only slowly converge to their asymptotic estimates. This indicates that the asymptotics are only valid for large $N > 1000$.

## References


[1] Moortgat K T, Keller C H, Bullock T H and Sejnowski T J 1998 Submicrosecond pacemaker precision is behaviorally modulated: the gymnotiform electromotor pathway *Proc. Natl Acad. Sci. USA* **95** 4684–9

[2] Moortgat K T, Bullock T H and Sejnowski T J 2000 Precision of the pacemaker nucleus in a weakly electric fish: network versus cellular influences *J. Neurophysiol.* **83** 971–83

[3] Moortgat K T, Bullock T H and Sejnowski T J 2000 Gap junction effects on precision and frequency of a model pacemaker network *J. Neurophysiol.* **83** 984–97

[4] Knight B W 1972 Dynamics of encoding in a population of neurons *J. Gen. Physiol.* **59** 734–66

[5] Knight B W 1972 The relationship between the firing rate of a single neuron and the level of activity in a population of neurons. Experimental evidence for resonant enhancement in the population response *J. Gen. Physiol.* **59** 767–78

[6] Needleman D J, Tiesinga P H E and Sejnowski T J 2001 Collective enhancement of precision in networks of coupled oscillators *Physica* D at press

[7] Mainen Z F and Sejnowski T J 1995 Reliability of spike timing in neocortical neurons *Science* **268** 1503–6

[8] Reichl L E 1998 *A Modern Course in Statistical Physics* 2nd edn (New York: Wiley) p 199

[9] Press W H, Teukolsky S A, Vetterling W T and Flannery B P 1992 *Numerical Recipes* 2nd edn (Cambridge: Cambridge University Press)

[10] Hansel D, Mato G, Meunier C and Neltner L 1998 On numerical simulations of integrate-and-fire neural networks *Neural Comput.* **10** 467–83

[11] van Vreeswijk C, Abbott L F and Ermentrout G B 1994 When inhibition not excitation synchronizes neural firing *J. Comput. Neurosci.* **1** 313–22

[12] Terman D and Wang D L 1995 Global competition and local cooperation in a network of neural oscillators *Physica* D **81** 148–76

[13] Hansel D, Mato G and Meunier C 1995 Synchrony in excitatory neural networks *Neural Comput.* **7** 307–37

[14] Gerstner W, van Hemmen J L and Cowan J 1996 What matters in neuronal locking? *Neural Comput.* **8** 1653–76

[15] Abbott L F, Varela J A, Sen K and Nelson S B 1997 Synaptic depression and cortical gain control *Science* **275** 220–4

[16] Markram H, Wang Y and Tsodyks M 1998 Differential signaling via the same axon of neocortical pyramidal neurons *Proc. Natl Acad. Sci. USA* **95** 5323–8

[17] Keener J, Hoppensteadt F and Rinzel J 1981 Integrate-and-fire models of nerve membrane response to oscillatory input *SIAM J. Appl. Math.* **41** 503–17

[18] Tateno T 1998 Characterization of stochastic bifurcations in a simple biological oscillator *J. Stat. Phys.* **92** 675–705

[19] Coombes S and Bressloff P C 1999 Mode locking and Arnold tongues in integrate-and-fire neural oscillators *Phys. Rev.* E **60** 2086–96

[20] Tateno T and Jimbo Y 2000 Stochastic mode-locking for a noisy integrate-and-fire oscillator *Phys. Lett.* A **271** 227–36

[21] Longtin A and Chialvo D R 1998 Stochastic and deterministic resonances for excitable systems *Phys. Rev. Lett.* **81** 4012–5

[22] Tiesinga P H E and José, J V 2000 Robust gamma oscillations in networks of inhibitory hippocampal interneurons *Network* **11** 1–23

[23] Hunter J D, Milton J G, Thomas P J and Cowan J D 1998 Resonance effect for neural spike time reliability *J. Neurophysiol.* **80** 1427–38

[24] Tiesinga P H E, Fellous J-M, José J V and Sejnowski T J 2001 Optimal information transfer in synchronized neocortical neurons *Neurocomputing* **38–40** 397–402

[25] Larsen R J and Marx M L 1986 *An Introduction to Mathematical Statistics and its Applications* 2nd edn (Englewood Cliffs, NJ: Prentice-Hall) p 146